

Pseudolabel guided pixels contrast for domain adaptive semantic segmentation

Jianzi Xiang, Cailu Wan, and Zhu Cao*

The Key Laboratory of Smart Manufacturing in Energy Chemical Process, Ministry of Education, East China University of Science and Technology, Shanghai 200237, China

**Corresponding author email: caozhu@ecust.edu.cn*

Abstract

Semantic segmentation is essential for comprehending images, but the process necessitates a substantial amount of detailed annotations at the pixel level. Acquiring such annotations can be costly in the real-world. Unsupervised domain adaptation (UDA) for semantic segmentation is a technique that uses virtual data with labels to train a model and adapts it to real data without labels. Some recent works use contrastive learning, which is a powerful method for self-supervised learning, to help with this technique. However, these works do not take into account the diversity of features within each class when using contrastive learning, which leads to errors in class prediction. We analyze the limitations of these works and propose a novel framework called *Pseudo-label Guided Pixel Contrast* (PGPC), which overcomes the disadvantages of previous methods. We also investigate how to use more information from target images without adding noise from pseudo-labels. We test our method on two standard UDA benchmarks and show that it outperforms existing methods. Specifically, we achieve relative improvements of 5.1% mIoU and 4.6% mIoU on the Grand Theft Auto V (GTA5) to Cityscapes and SYNTHIA to Cityscapes tasks based on DAFormer, respectively. Furthermore, our approach can enhance the performance of other UDA approaches without increasing model complexity. Code is available at <https://github.com/embar111/pgpc>

Keywords: Semantic Segmentation, Unsupervised Domain Adaptation, Contrastive Learning

1. Introduction

Semantic segmentation, assigning semantic labels to pixels, is crucial for applications like medical analysis [1], robot navigation [2], and autopilot [3]. In the preceding years, numerous methods founded on Convolutional Neural Networks (CNN) [4–8] and Transformers [9–12] have been proposed and obtained surprising effects. However, these methods rely on a mass of expensive and labor-intensive pixel-level labels thus hindering their practical applicability. One alternative to solve this problem is training semantic segmentation networks using virtual datasets [13, 14] that can automatically obtain pixel-level labels. Therefore, the problem of eliminating the domain gap between virtual (source domain) and real (target domain) images, known as UDA on semantic segmentation, has garnered significant interest among researchers.

Recent works for UDA attempt to learn the common domain-invariant knowledge through two methods: adversarial learning [15] and self-training [16–21]. Adversarial learning aligns global distributions between the source and target domain by deceiving a domain discriminator, but it fails to ensure the separability of features across different categories in the target domain [22]. Self-training methods, which adopted confidence estimation [23], consistency regularization [24], or entropy minimization [25]

to improve the segmentation performance, utilize pseudo-labels to enable a class-wise alignment. Despite the good performance of these methods, they mostly do not accurately bridge domain discrepancies, resulting in indistinct target representations [26]. To address the problem described above, motivated by the success of contrastive learning [27] whose objective is to separate dissimilar (negative) data pairs and align similar (positive) data pairs in the self-supervised learning, some recent works [26, 28–31] apply contrastive learning to the UDA on semantic segmentation and obtain good results.

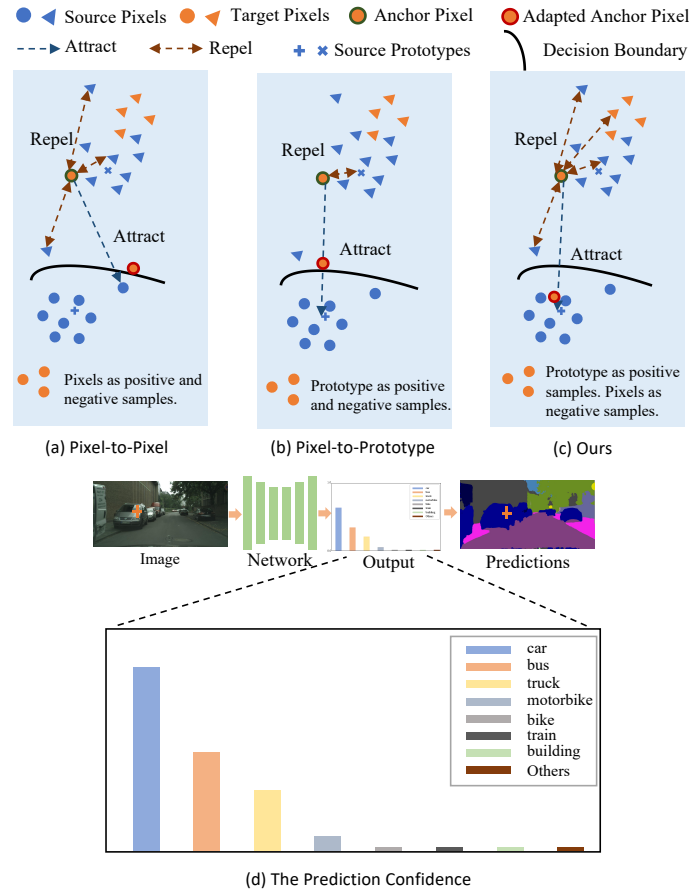


Figure 1: The schematic diagram of our motivation. (a) and (b) are the pixel-to-pixel and pixel-to-prototype contrastive learning methods, respectively. (c) is our contrastive learning method. (d) is the prediction confidence of the pixel marked with an orange cross. The adapted anchor pixel means the anchor pixel is trained by contrastive learning. The adapted anchor pixel is misplaced on the incorrect side of the decision boundary in (a) and (b), while (c) correctly positions it on the right side.

Currently, there exist opportunities for enhancement in two aspects of these contrastive methods: the modality of contrastive learning and the utilization of pseudo-labels. On the one hand, contrastive learning in UDA for semantic segmentation primarily employs two methodological approaches: pixel-to-pixel and pixel-to-prototype. The pixel-to-pixel methods [26, 30] use contrastive learning to narrow the gap within pixel-wise feature representations for pixels sharing the same class, while simultaneously widening the separation for those belonging to distinct classes, irrespective of the domain. However, these methods do not guarantee that the pixel representations are close to the feature center of their category, because the pixel representations are scattered in different spatial locations, as shown in Fig. 1(a). The pixel-to-prototype methods [28, 31] use contrastive learning to

reduce the discrepancies between pixel representations and their respective category prototypes, which are the feature centers of each category. These methods are effective in tackling the challenges faced by pixel-to-pixel methods, but they do not separate the pixel representations of different categories well enough across domains. This is because each category has a large diversity of pixel representations, and the feature boundaries of each category may be far from the category prototypes. Even when the pixel features of one class have been distanced from the prototypes of other classes, they might still reside within the feature spaces of those other classes, as depicted in Fig. 1(b). So the above two types of contrastive learning methods may still fail to learn distinguishable representations.

Conversely, the process of semantic segmentation necessitates pixel-wise guidance for the execution of contrastive learning. However, target images do not have ground-truth labels, so previous methods use pseudo-labels generated from predictions to perform contrastive learning at the pixel level. Some methods [28] use all predictions as pseudo-labels without filtering out noisy pseudo-labels, which can degrade the model performance. To avoid confirmation bias [32] and reduce the effect of incorrect pseudo-labels, some methods [29] use a class-wise adaptive thresholding method to select only confident predictions as pseudo-labels and ignore uncertain ones. But insufficient use of pixels in the target image can also lead to degradation of the final performance. Our method selects reliable predictions as pseudo-labels, thereby minimizing the influence of noise. With each training iteration, the model updates its predictions, yielding even more credible pseudo-labels. Through this iterative process, spanning the entire training duration, the model harnesses an increasingly vast array of pixels for learning, ultimately enhancing its overall performance. As a prominent approach within unsupervised learning, our pseudo-label methodology prioritizes utilizing the utmost quantity of reliable pseudo-label samples as training data, thereby offering a valuable benchmark for subsequent endeavors in this domain.

Through these analyses, we introduce an innovative framework that integrates both the pixel-to-pixel and pixel-to-prototype methods first. Specifically, our method makes use of class prototypes as positive instances to reduce their distance from the prototype of the same category in the source domain for each target pixel representation of a certain category, and pixels to increase its distance to some random source pixel representations of other categories. By integrating the pixel-to-pixel method with the pixel-to-prototype approach, our model gains the capability to not only discern pixel representations and the distinctions between pixels belonging to diverse categories but also capture the similarities between pixel representations and the prototypes of the same category. Then, we propose a method that leverages all target pixels in contrastive learning for UDA. The method is derived from the assumption that the model can differentiate between dissimilar classes and only confuse a few classes that are similar. In particular, as indicated in Fig. 1(d), a pixel may have similar probabilities for class *car*, *bus*, and *truck*. But the model confidently rejects class *person*, *vegetable*, and other classes. So we can use this pixel as a negative sample for class *person* or *vegetable*. We combine this method with our proposed framework to achieve better results. For example, as shown in Fig. 1(c), our method reduces the distance between the anchor pixel and positive samples (prototype), while increasing the distance to negative samples (pixels), so that it is classified as the correct category. This approach enables the simultaneous consideration of both the wide distribution of pixels in the feature space and the excessive distance between prototypes and decision boundaries. Below is a detailed account of the primary contributions made by our study:

- We propose a new contrastive learning framework for UDA on semantic segmentation by integrating the pixel-to-pixel and pixel-to-prototype methods.
- We introduce a novel approach, which can utilize all target pixels effectively in our proposed framework.
- We perform comprehensive evaluations on renowned UDA benchmarks, specifically the GTA5 to Cityscapes and Synthia to Cityscapes transitions. Our approach has demonstrated significant improvements across various advanced UDA frameworks. For example, we attain relative improvements of 5.1% mIoU and 4.6% mIoU on the two UDA benchmarks based on DAFormer, respectively.

2. Related Work

2.1. Semantic Segmentation

The field of semantic segmentation has experienced remarkable progress since Long *et al.* [33] utilized CNN for this task. A common challenge for semantic segmentation is to capture large-scale contextual information, which requires large receptive fields. In response to this issue, numerous strategies have been put forward, such as context aggregation [34, 35], attention modules [36–38], and atrous convolution [4, 5]. Complementing CNN-based techniques, the Transformer-based methods have received considerable attention from researchers in recent times. These Transformer-based [39] models have demonstrated exceptional efficacy in the realm of natural language processing, and have inspired recent efforts to apply them to visual tasks [10, 11, 40, 41]. One of the pioneering methods in this direction is SETR [10] which adopts a sequence-to-sequence approach and uses ViT [40], a framework purely based on Transformers, as its core for extracting features from image tokens. ViT divides an image into token sequences and processes them with a series of Transformer encoders, demonstrating the effectiveness of Transformers for visual recognition. Moreover, Swin Transformer [41] introduces a hierarchical Transformer that can capture multiscale visual information and adapt to the differences between language and vision domains. SegFormer [11] designs an innovative encoder with a hierarchical Transformer architecture that produces features across various scales and a lightweight decoder that combines them into a powerful representation. These Transformer-based methods consistently achieve remarkable results on semantic segmentation.

2.2. Unsupervised Domain Adaptation

Unsupervised domain adaptation is a technique that uses virtual data with labels to train a model and adapts it to real data without labels. Semantic segmentation requires a substantial number of pixel-level annotations, but acquiring these annotations in the real world can be quite costly, so UDA is suitable for semantic segmentation that require a large amount of pixel-level annotations. The landscape of UDA techniques for semantic segmentation typically encompasses two primary strategies: methods grounded in adversarial training and those based on self-training approaches. Adversarial training approaches regard the segmentation modules as generators that try to produce domain-invariant features [42] or predictions [15] for images from different domains, while discriminators are utilized to identify the domain of the features or predictions. Alternatively, UDA can

be achieved through the process of imparting the visual aesthetics of source domain to the target domain, leveraging the principles of adversarial training as referenced in [43, 44]. Self-training techniques are designed to generate pseudo-labels for target images, leveraging a network trained on labeled source images. However, domain discrepancy inevitably introduces noise into these pseudo-labels. In response to this challenge, numerous strategies have been put forward, such as confidence thresholding [45, 46], consistency regularization [24, 47], domain-mixup [48, 49], and pseudo-labels rectification [17, 50]. Self-training methods have emerged as the dominant methods in UDA due to their stability and superior performance. DAFormer [51] is the first method to integrate the Transformer architecture and self-training for UDA. To ensure a stable training process and prevent overfitting to the source domain, DAFormer employs three simple yet effective training strategies. Building on this work, HRDA [52] leverages high-quality and low-quality images to enhance the segmentation results through a scale attention module, leading to top-tier performance levels.

2.3. Contrastive Learning

The contrastive learning approach [27] aims to minimize the differences in features among similar instances, while simultaneously maximizing the distinctions between dissimilar ones. It is a key component of metric learning and has been widely used in self-supervised learning [53–55]. Some recent works [56–60] have applied contrastive learning for semantic segmentation with pixel-level labels in either a fully supervised or a semi-supervised setting. These methods have achieved favorable outcomes in both fully supervised and semi-supervised domains. Using these techniques, one can extract more robust and discriminative features. However, since these methods do not account for cross-domain adaptation concerns, they cannot be readily applied in unsupervised domains. Hence, several investigations have explored integrating contrastive learning in unsupervised semantic segmentation and have achieved notable performance. Currently, there are three types of methods: pixel-to-pixel [26, 30], pixel-to-prototype [28, 31], and prototype-to-prototype [29]. These methods are capable of reducing domain discrepancies while simultaneously enhancing the discriminability among different categories.

3. Method

Below, Section 3.1 introduces the mathematical framework that defines the issue at hand and an overview of PGPC. Section 3.2 describes the strategy for selecting reliable target image pixels. Section 3.3 explains the specific contrastive learning algorithm of PGPC.

3.1. Overview

Considering the problem of UDA for semantic segmentation involves a collection of source images $\mathcal{X}_s = \{x_s^i\}_{i=1}^{N_s}$ from the virtual-world with C -class segmentation labels $\mathcal{Y}_s = \{y_s^i\}_{i=1}^{N_s}$, and a collection of target images $\mathcal{X}_t = \{x_t^i\}_{i=1}^{N_t}$ from the real-world without any labels. We aim to develop a neural network model capable of utilizing the source data to boost the precision of segmentation when applied to target data.

Subsequently, the student model Θ is fine-tuned on the target domain using the CE loss function with the guidance of pseudo-labels:

$$\mathcal{L}_t = - \sum_{j=1}^{H \times W} \sum_{c=1}^C q_T^{(j)}(p_t^{i(j,c)}) \log \Theta(x_t^{i(j,c)}). \quad (4)$$

Within the framework of self-training, we employ the contrastive loss to improve the feature discriminability among diverse classes. \mathcal{L}_c is the pixel-wise InfoNCE [61] computed as:

$$\mathcal{L}_c = - \frac{1}{C \times M} \sum_{c=0}^{C-1} \sum_{m=1}^M \log \left[\frac{e^{\langle z_{cm}, z_c^+ \rangle / \tau}}{e^{\langle z_{cm}, z_c^+ \rangle / \tau} + \sum_{n=1}^N e^{\langle z_{cm}, z_{cmn}^- \rangle / \tau}} \right]. \quad (5)$$

It shows that we use contrastive learning to train our model on M anchor pixels from class c , each paired with one positive sample and N negative samples. We denote the representations of the m -th anchor pixel and positive sample as z_{cm} and z_c^+ where z is the output of the projection head. z_{cmn}^- denotes the n -th negative sample of the m -th anchor pixel. We measure the distance between features from different pixels by cosine similarity $\langle \cdot, \cdot \rangle$ and use a temperature parameter τ to learn from hard negatives. In the pixel-to-pixel methods, both positive and negative samples consist of pixel representations. In the pixel-to-prototype methods, both positive and negative samples are class prototypes. Contrary to these approaches, our technique employs class prototypes as positive and pixel representations as the negative instances. The merits of our approach have been elucidated in the introduction. Moreover, previous methods do not optimally exploit every pixel representation within the target domain. Conversely, our approach effectively integrates all target pixel representations into the contrastive learning during training. To employ the contrastive loss, we first need to select reliable target image pixels, and then utilize the source image annotations and target image pseudo-labels to determine and calculate the components required for contrastive learning. This matter will be elaborated upon in greater detail in the following sections, namely Section 3.2 and Section 3.3.

To sum up, the aim of optimization is to lower all encompassed losses, delineated mathematically as:

$$\mathcal{L} = \mathcal{L}_s + \lambda_t \mathcal{L}_t + \lambda_c \mathcal{L}_c, \quad (6)$$

where λ_t is the weight of target domain loss, and λ_c is the weight of contrastive loss. Moreover, the contrast loss is computed following a specified number of warmup iterations to maintain training stability.

3.2. Selecting Reliable Target Image Pixels

We employ per-pixel prediction entropy to filter high confident pixels for contrastive learning, which mitigates the negative influence of inaccurate pseudo-labels. Specifically, for pixel j of each i -th target image, $(P_t^i)^j$ is used to denote the softmax

probabilities as output by the segmentation head of the teacher model. The entropy is calculated by:

$$(E_t^i)^j = - \sum_{c=0}^{C-1} (P_t^i)^j_c \log(P_t^i)^j_c, \quad (7)$$

where C signifies the tally of distinct classes and $(P_t^i)^j_c$ corresponds to the c -th component of $(P_t^i)^j$. We consider pixels whose entropy is in the lowest $\eta\%$ as confident pixels. $\eta\%$ is a hyperparameter that will be determined through experiments. Specifically, we set the threshold γ_t , such that the fraction of elements in E_t^i that are lower than γ_t , is equal to $\eta\%$.

3.3. Contrastive Learning

By employing contrastive learning, our proposed approach aims to improve the feature discrimination among different target classes, visualized in Fig. 3. It is made up of three components: anchor pixels, positive samples, and negative samples. Note that for efficiency, anchor pixels and negative samples are sourced from certain sets, thus reducing computational costs. We describe these three components in the following paragraphs.

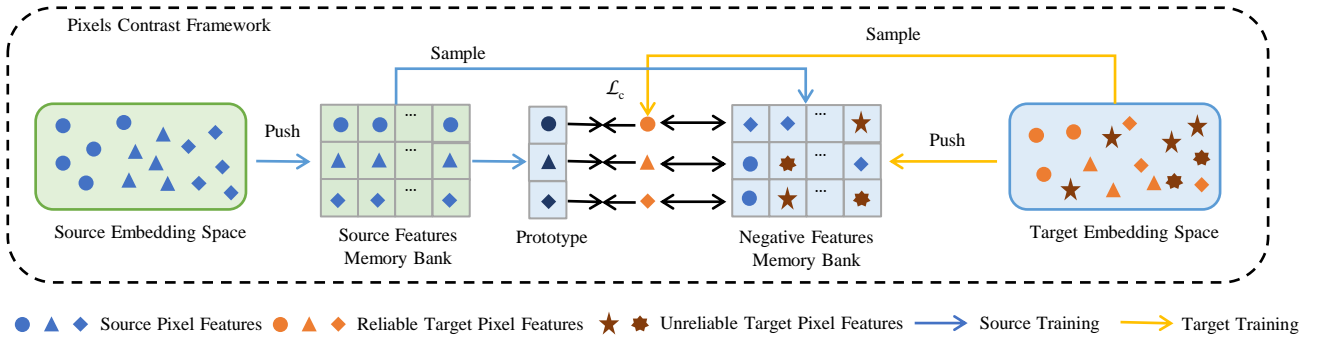


Figure 3: An overview of pixels contrast framework. Reliable target pixel features are sampled from the target embedding space, followed by decreasing the distance between these features and class prototypes while concurrently increasing the distance between them and negative features. To fully leverage the pixels from target images, unreliable target pixel features are introduced into the contrastive learning during training.

Anchor Pixels. In contrastive learning, anchor pixels serve as the starting points for constructing pairs of positive and negative samples and are utilized to guide feature learning. For every class within the current mini-batch, we select corresponding anchor pixels during training. Features from all candidate anchor pixels for category c are encapsulated within the set \mathcal{A}_c :

$$\mathcal{A}_c = \{(z_t^i)^j \mid (p_t^i)^j = c \cap (E_t^i)^j < \gamma_t\}, \quad (8)$$

where $(p_t^i)^j$ and $(z_t^i)^j$ denote the pseudo-label and corresponding representation for pixel j within the target image i , respectively.

Positive Samples. We utilize the prototype of each class as the positive sample in our method. To bring the prototype closer to the potential feature distribution center of class c , we utilize not only the current mini-batch pixel representations but also a memory bank to compute the prototype. This memory bank can store a collection of pixel representations of class c , allowing

access to a broader range of representations for calculating the prototype:

$$z_c^+ = \frac{1}{|\mathcal{M}_c|} \sum_{z_c \in \mathcal{M}_c} z_c, \quad (9)$$

where \mathcal{M}_c denote all the source pixel representations for category c within the memory bank. Note that the prototype of category c is used for all anchor pixels assigned to the category c .

Negative Samples. Negative Samples are included from two distinct realms: the source domain and the target domain. When considering i -th image of the source domain, a qualified negative sample of category c is defined as one that does not fall within category c . Specifically, the collection of negative samples in source images for class c is

$$\mathcal{N}_s^c = \{(z_s^i)^j \mid (y_s^i)^j \neq c\}. \quad (10)$$

On the other hand, with the objective of capitalizing on the information contained within all target pixels for improved discrimination, we operate under the assumption that the model can effectively distinguish between dissimilar classes while potentially encountering confusion primarily among a subset of classes that exhibit similarity. For instance, as depicted in Fig. 1(d), the pixel marked with an orange cross exhibits comparable probabilities for belonging to classes such as *car*, *bus*, and *truck* while the model exhibits a high level of confidence in rejecting classes like *person*, *vegetable*, and other similar classes. Consequently, we can utilize this pixel as a negative sample for classes like *person* or *vegetable*. In this context, we define a qualified negative sample of category c concerning the i -th target image as one characterized by a low probability of being associated with category c . To achieve this, we define the pixel-level category order O_{ij} as the sorted indices of $(P_t^i)^j$ in ascending order. It follows that $O_{ij}(\operatorname{argmax}(P_t^i)^j) = 0$ and $O_{ij}(\operatorname{argmin}(P_t^i)^j) = C - 1$, where C signifies the total count of distinct classes present. Then the set of negative samples in target images for class c is

$$\mathcal{N}_t^c = \{(z_t^i)^j \mid \mathbb{1}[O_{ij}(c) \geq r] = 1\}, \quad (11)$$

where $\mathbb{1}$ is the notation for an indicator function and r is established as 4 to filter out features that have a low probability of belonging to class c . However, the quantity of negatives is constrained by the mini-batch size, which hinders the contrastive representation learning [62]. Therefore, we adopt large and external memories as a bank to store more negative samples of class c , following [62]. Moreover, the stored negative samples are updated dynamically through a momentum-updated mechanism.

After obtaining these components, we can calculate the contrastive loss according to Eq. (5). Algorithm 1 provides a structured overview of the principal stages of our technique.

4. Experiments

This section elaborates on the experimental setup, encompassing datasets, metrics for evaluation, utilized architectures, and implementation details. Subsequently, it exhibits the outcomes of our proposed approach and demonstrates its effectiveness.

Algorithm 1: PGPC

input : Source data $\mathcal{X}_s, \mathcal{Y}_s$, target data \mathcal{X}_t , and hyperparameters.
output: Final network weights Θ .

```
1 Initialize student  $\Theta$  and teacher  $\Theta'$  model parameters;  
2 for iteration  $\leftarrow 0$  to total iterations do  
3   Randomly sample source images  $\mathcal{B}_s$  and target images  $\mathcal{B}_t$ ;  
4   Compute target image predictions  $p_t$  using teacher model;  
5   if iteration > warmup iterations then  
6     Separate pixel-level representation of both domains in the embedding space;  
7     Get anchor pixels  $z_{cm}$  from  $\mathcal{A}_c$ ;  
8     Get negative samples  $z_{cmn}^-$  from  $\mathcal{N}_s^c$  and  $\mathcal{N}_t^c$ ;  
9     Get positive samples  $z_c^+$  based on Eq. (9);  
10    Compute contrastive loss  $\mathcal{L}_c$  based on Eq. (5);  
11    Compute loss for the mini-batch  $\mathcal{L}$  based on Eq. (6) and backpropagation;  
12    Update  $\Theta$  and  $\Theta'$ .
```

4.1. Experimental Details

Datasets. The Cityscapes dataset [63] encompasses a collection of 5,000 images, each with pixel-wise semantic annotations, alongside 20,000 images featuring broader semantic annotations. These visual data are collected from 50 different real-world cities. The target domain is composed of 2975 unlabeled images from the Cityscapes training dataset. To gauge the efficacy of our model, its performance is meticulously assessed using a separate set of 500 images from the Cityscapes validation dataset, which benefits from comprehensive labeling.

The GTA5 dataset [13] has 24,966 computer-generated images originating from a virtual gaming engine. The network is trained on 19 classes that are common between GTA5 and Cityscapes, and the rest of the classes are ignored.

The SYNTHIA dataset [14], a virtual compilation of imagery, includes 9,400 urban scenes with high-quality masks. It is used to train the network on 13 classes that correspond to those found in the Cityscapes dataset.

Evaluation. The mean intersection-over-union (mIoU) metric, a standard in UDA for semantic segmentation, is utilized to assess the efficacy of semantic segmentation networks.

Architectures. The implementation of our approach follows the recent advanced UDA setting and is based on the DAFormer [51]. We also adopt HRDA [52] to further substantiate the efficacy of our approach. Specifically, we utilize the MiT-B5 encoder [11] pretrained on ImageNet-1k [64] to generate a feature pyramid with $\mathcal{F}_d = [64, 128, 320, 512]$. The features are passed on a segmentation head and a projection head. The segmentation head aligns with the configuration of the decoder in DAFormer [51] that uses a multitude of multiple 3×3 depthwise separable convolutions operating in parallel and characterized by a spectrum of dilation rates. Concurrently, the projection head facilitates the transformation of high-dimensional pixel embeddings into a feature vector of 256 dimensions, normalized through the l_2 scheme. Furthermore, in the context of HRDA [52], an additional scale attention head is implemented, which parallels the streamlined MLP-based decoder of the SegFormer model [11], with an embedding dimension also set to 256.

Implementation details. Experiments are conducted using PyTorch and are based on the mmsegmentation toolbox [65].

We adopt the training approach as DAFormer [51] and HRDA [52] and use AdamW [66] optimizer, characterized by betas (0.9, 0.999) and a weight decay of 0.01. Moreover, the learning rate of the encoder is configured to 6×10^{-5} , while 6×10^{-4} is the designated learning rate for the segmentation head and the projection head. For self-training, we keep $\alpha = 0.999$ as the EMA weight update parameter and apply three training strategies: linear learning rate warmup policy, rare class sampling, and feature distance regularization. Throughout the training phase, we train our semantic segmentation network for 60k iterations. Moreover, for an equitable comparison, we set κ to 0.968 following DAFormer [51]. For the contrastive learning, we selected the values of the warmup iterations and the temperature parameter τ based on the literature and our preliminary experiments. Specifically, we used 20k warmup iterations and $\tau = 0.5$. We tuned the other hyperparameters empirically to optimize the performance of our model.

4.2. Experimental Results

We execute an in-depth examination of our approach against the advanced approaches [28, 51, 52] within two exemplary virtual-to-real adaptation tasks: GTA5 to Cityscapes, SYNTHIA to Cityscapes, Cityscapes to DarkZurich and Cityscapes to Adverse Conditions Dataset with Correspondences (ACDC). The quantitative results are presented in Tables 1 and 2. Qualitative results of the segmentation effectiveness are illustrated in Figure 4. Our method is validated to secure outstanding segmentation performance in each scenario, using different segmentation models such as DAFormer [51] and HRDA [52].

GTA5 to Cityscapes. TABLE 1 exhibits the adaptation results on the task of GTA5 to Cityscapes, where we compare our approach with the advanced UDA approaches [26, 28, 29, 67]. Optimal results are denoted with bold formatting. Our method achieves a leading result of 71.8 mIoU, which significantly surpasses DAFormer by +3.5 mIoU. This indicates that our method can effectively leverage contrastive learning and pixel-level alignment to improve the domain adaptation performance. Moreover, when we apply our method to HRDA, we further boost the mIoU by +1.2 mIoU, demonstrating the scalability and robustness of our method to different segmentation models.

SYNTHIA to Cityscapes. TABLE 2 showcases the adaptation outcomes on SYNTHIA to Cityscapes. Our approach yields a mIoU score of 67.7, rivaling the performance of advanced approaches such as SePiCo [28] and CLUDA [26]. In addition, our method outperforms them in some challenging classes. This shows that our approach successfully extends its applicability to different virtual-to-real adaptation scenarios and captures the semantic features of the target domain.

Cityscapes to DarkZurich. TABLE 3 shows the outcomes of Cityscapes to DarkZurich. Our method achieved the best performance of 61.2 mIoU, improving by 1.1 mIoU compared to MIC (HRDA) [68]. Moreover, our method demonstrates better domain adaptation capabilities, for example, in the class *bus*, our method improved by 35.1% compared to the previous best approach, MIC (HRDA) [68].

Cityscapes to ACDC. We test different models on Cityscapes to ACDC task, and the result is shown in Table 4. Our method achieve 71.4 mIoU, which is an increase of 1.0 mIoU compared to the best past method, MIC (HRDA) [68]. In harsh environmental conditions, our method still performed at its best, indicating that our approach has a certain degree of robustness against interference.

Qualitative results. Fig. 4 illustrates some segmentation examples and compares them with the ground truth and the predictions of SePiCo [28], DAFormer [51], and HRDA [52]. We use colored boxes to indicate the regions where our method can segment minor categories better than the other methods. The proficiency of our method in generating precise segmentation is evident for minority classes, with sharper and more accurate boundaries between categories.

The speed and complexity. Our method integrates contrastive learning with DAFormer [51], which does not increase model complexity but increases training time and inference time. Table 5 presents the training speed and inference speed of various methods. In the Cityscapes to Darkzurich task, training a single image with PGPC + DAFormer takes 33% longer compared to DAFormer, while PGPC + HRDA shows a 33% increase in training time relative to HRDA [52]. The inference speed of PGPC + HRDA is not different from HRDA[52], but PGPC + DAFormer takes 3.6 times as long as DAFormer.

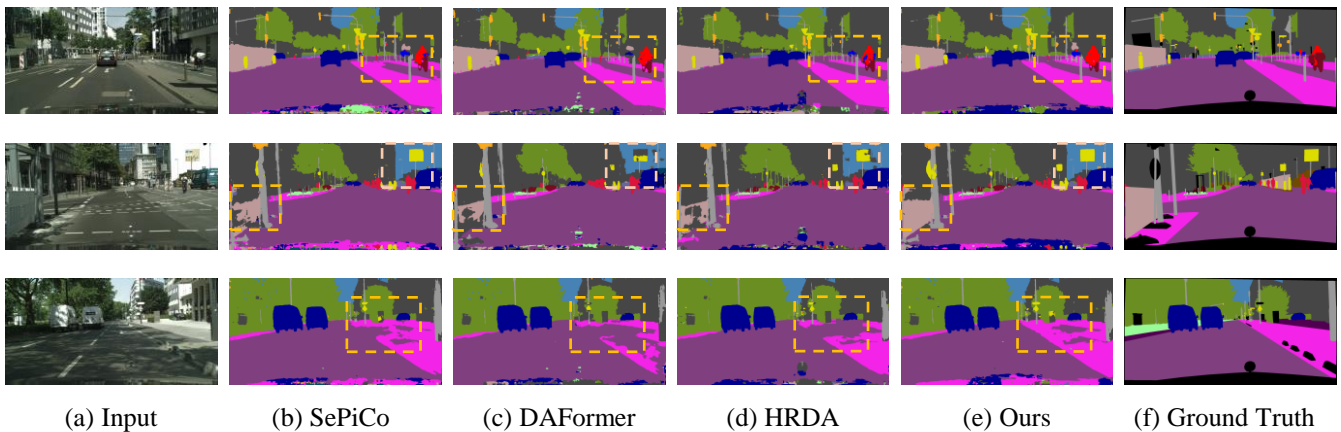


Figure 4: Qualitative examples of semantic segmentation on the GTA5 to Cityscapes. (a) and (f) are the images and the ground truth labels from the Cityscapes validation dataset. (b), (c), and (d) are the segmentation predictions of SePiCo [28], DAFormer [51], and HRDA [52]. (e) are the segmentation outputs of our method. We emphasize areas of superior performance by our method with highlighted colored boxes.

4.3. Ablation Studies and Further Discussion

Effectiveness of the contrastive learning. To evaluate the influence of contrastive learning on the domain adaptation task of GTA5 to Cityscapes, we conduct our experiments using the same setup and hyperparameters as the DAFormer [51]. Table 6 shows that contrastive learning can improve the mIoU by +3.5 compared with the baseline. Moreover, our experimental approach includes assessing how different selections of positive and negative samples affect the performance. Table 6 reveals that using target negative pixels contributes to a significant increase in mIoU. This affirms our viewpoint that the comprehensive potential of target images can be fully realized through the optimization of individual pixel utilization. In addition, using source prototypes rather than target prototypes as positive samples can better narrow the domain gap, thereby achieving improved results. From Table 6 and Table 1, even without incorporating the use of all target pixels, our proposed framework (70.8 mIoU)

Table 1: The mIoU % scores of semantic segmentation models trained on GTA5 and evaluated on the Cityscapes validation dataset. The preeminent scores within columns are highlighted through bold text.

GTA5 to Cityscapes																				
Method	road	sidewalk	building	wall	fence	pole	light	sign	veg	terrain	sky	person	rider	car	truck	bus	train	mbike	bike	mIoU
IAST[45]	94.1	58.8	85.4	39.7	29.2	25.1	43.1	34.2	84.8	34.6	88.7	62.7	30.3	87.6	42.3	50.3	24.7	35.2	40.2	52.2
UncerDA[17]	90.5	38.7	86.5	41.1	32.9	40.5	48.2	42.1	86.5	36.8	84.2	64.5	38.1	87.2	34.8	50.4	0.2	41.8	54.6	52.6
DACS[69]	89.9	39.7	87.9	30.7	39.5	38.5	46.4	52.8	88.0	44.0	88.8	67.2	35.8	84.5	45.7	50.2	0.0	27.3	34.0	52.1
SAC[70]	90.4	53.9	86.6	42.4	27.3	45.1	48.5	42.7	87.4	40.1	86.1	67.5	29.7	88.5	49.1	54.6	9.8	26.6	45.3	53.8
ProCA[29]	91.9	48.4	87.3	41.5	31.8	41.9	47.9	36.7	86.5	42.3	84.7	68.4	43.1	88.1	39.6	48.8	40.6	43.6	56.9	56.3
BCL[31]	93.5	60.2	88.1	31.1	37.0	41.9	54.7	37.8	89.9	45.5	89.9	72.7	38.2	90.7	34.3	53.2	4.4	47.2	58.5	57.1
ProDA[67]	87.8	56.0	79.7	46.3	44.8	45.6	53.5	53.5	88.6	45.2	82.1	70.7	39.2	88.8	45.5	59.4	1.0	48.9	56.4	57.5
CaCo[30]	93.8	64.1	85.7	43.7	42.2	46.1	50.1	54.0	88.7	47.0	86.5	68.1	2.9	88.0	43.4	60.1	31.5	46.1	60.9	58.0
DAFormer[51]	95.7	70.2	89.4	53.5	48.1	49.6	55.8	59.4	89.9	47.9	92.5	72.2	44.7	92.3	74.5	78.2	65.1	55.9	61.8	68.3
CLUDA+DAFormer[26]	97.5	78.8	88.8	60.8	52.0	47.1	51.9	50.3	89.7	51.0	94.0	71.0	48.6	93.1	82.0	84.1	71.4	58.9	60.7	70.1
SePiCo[28]	96.9	76.7	89.7	55.5	49.5	53.2	60.0	64.5	90.2	50.3	90.8	74.5	44.2	93.3	77.0	79.5	63.6	61.0	65.3	70.3
MIC(DAFormer)[68]	96.7	75.0	90.0	58.2	50.4	51.1	56.7	62.1	90.2	51.3	92.9	72.4	47.1	92.8	78.9	83.4	75.6	54.2	62.6	70.6
HRDA[52]	96.4	74.4	91.0	61.6	51.5	57.1	63.9	69.3	91.3	48.4	94.2	79.0	52.9	93.9	84.1	85.7	75.9	63.9	67.5	73.8
CLUDA+HRDA[26]	97.1	78.0	91.0	60.3	55.3	56.3	64.3	71.5	91.2	51.1	94.7	78.4	52.9	94.5	82.8	86.5	73.0	64.2	69.7	74.4
PDA[18]	97.8	78.1	92.4	70.8	53.1	58.5	58.2	67.1	92.0	54.4	94.8	81.4	54.5	92.9	86.9	87.1	78.6	68.1	69.7	75.6
MIC(HRDA)[68]	97.4	80.1	91.7	61.2	56.9	59.7	66.0	71.3	91.7	51.4	94.3	79.8	56.1	94.6	85.4	90.3	80.4	64.5	68.5	75.9
PGPC+ProCA	93.1	51.6	89.4	44.7	40.5	49.2	52.4	45.6	88.3	48.7	86.9	70.2	40.2	89.2	70.9	50.7	48.6	46.7	58.2	61.3
PGPC+DAFormer	97.1	77.4	90.2	56.8	51.7	53.9	61.2	66.8	90.4	50.0	93.0	74.6	41.5	93.4	80.5	85.4	78.6	59.9	62.5	71.8
PGPC+MIC(DAFormer)	96.4	77.3	90.7	55.2	54.8	56.2	60.2	67.2	90.9	51.0	86.7	75.4	49.6	93.8	83.5	83.6	76.3	60.2	65.0	72.3
PGPC+HRDA	97.2	75.4	92.4	64.1	58.4	58.7	64.4	71.4	91.7	53.4	94.7	76.5	53.0	94.4	86.1	85.2	75.0	65.4	68.5	75.0
PGPC+MIC(HRDA)	97.5	80.7	92.8	63.7	59.3	58.1	65.3	71.9	92.4	53.0	95.2	79.5	58.8	95.1	86.2	89.3	79.2	64.9	70.0	76.5

Table 2: The mIoU % scores of semantic segmentation models trained on SYNTHIA and evaluated on the Cityscapes validation dataset. The preeminent scores within columns are highlighted through bold text.

SYNTHIA to Cityscapes																	
Method	road	sidewalk	building	wall	fence	pole	light	sign	veg	sky	person	rider	car	bus	mbike	bike	mIoU
UncerDA[17]	79.4	34.6	83.5	19.3	2.8	35.3	32.1	26.9	78.8	79.6	66.6	30.3	86.1	36.6	19.5	56.9	48.0
IAST[45]	81.9	41.5	83.3	17.7	4.6	32.3	30.9	28.8	83.4	85.0	65.5	30.8	86.5	38.2	33.1	52.7	49.8
SAC[70]	89.3	47.2	85.5	26.5	1.3	43.0	45.5	32.0	87.1	89.3	63.6	25.4	86.9	35.6	30.4	53.0	59.3
ProCA[29]	90.5	52.1	84.6	29.2	3.3	40.3	37.4	27.3	86.4	85.9	69.8	28.7	88.7	53.7	14.8	54.8	53.0
ProDA[67]	87.8	45.7	84.6	37.1	0.6	44.0	54.6	37.0	88.1	84.4	74.2	24.3	88.2	51.1	40.5	45.6	55.5
BCL[31]	83.8	42.2	85.3	16.4	5.7	43.1	48.3	30.2	89.3	92.1	68.2	43.1	89.7	47.2	42.2	54.2	55.6
DAFormer[51]	84.5	40.7	88.4	41.5	4.5	53.1	55.0	54.6	86.0	89.8	73.2	48.2	87.2	53.2	53.9	61.7	60.9
CLUDA+DAFormer[26]	87.4	44.8	86.5	47.9	8.7	49.8	44.5	52.7	85.6	89.2	74.4	50.2	86.9	65.3	56.9	57.1	61.7
MIC(DAFormer)[68]	83.0	40.9	88.2	37.6	9.0	52.4	56.0	56.5	87.6	93.4	74.2	51.4	87.1	59.6	57.9	61.2	62.2
SePiCo[28]	87.0	52.6	88.5	40.6	10.6	49.8	57.0	55.4	86.8	86.2	75.4	52.7	92.4	78.9	53.0	62.6	64.3
HRDA[52]	85.2	47.7	88.8	49.5	4.8	57.2	65.7	60.9	85.3	92.9	79.4	52.8	89.0	64.7	63.9	64.9	65.8
PDA[18]	90.2	52.1	88.3	50.5	12.7	54.1	65.2	61.4	86.2	90.8	80.4	55.2	89.5	65.1	64.1	68.9	67.1
CLUDA+HRDA[26]	87.7	46.9	90.2	49.0	7.9	59.5	66.9	58.5	88.3	94.6	80.1	57.1	89.8	68.2	65.5	65.8	67.2
MIC(HRDA)[68]	86.6	50.5	89.3	47.9	7.8	59.4	66.7	63.4	87.1	94.6	81.0	58.9	90.1	61.9	67.1	64.3	67.3
PGPC+ProCA	87.4	54.0	86.1	40.8	5.4	47.3	46.7	30.4	89.4	88.1	70.8	35.7	85.4	57.6	40.4	58.9	57.8
PGPC+DAFormer	88.2	51.3	87.9	49.5	5.8	53.1	60.8	48.4	87.6	92.7	76.4	49.7	87.2	65.4	57.3	58.5	63.7
PGPC+MIC(DAFormer)	88.4	52.4	87.6	49.2	6.4	54.5	61.0	49.5	88.4	92.1	77.2	50.0	87.6	66.1	56.9	60.1	64.2
PGPC+HRDA	89.2	48.8	89.4	49.1	7.4	61.2	67.0	61.2	89.1	94.2	80.4	58.6	91.1	69.1	64.9	62.2	67.7
PGPC+MIC(HRDA)	89.4	53.5	89.4	49.7	6.7	63.1	68.4	60.5	89.7	93.9	80.8	59.2	91.4	68.5	65.4	64.9	68.4

Table 3: The mIoU % scores of semantic segmentation models trained on Cityscapes and evaluated on the DarkZurich test dataset. The preeminent scores within columns are highlighted through bold text.

Cityscapes to DarkZurich																				
Method	road	sidewalk	building	wall	fence	pole	light	sign	veg	terrain	sky	person	rider	car	truck	bus	train	mbike	bike	mIoU
ADVENT[71]	85.8	37.9	55.5	27.7	14.5	23.1	14.0	21.1	32.1	8.7	2.0	39.9	16.6	64.0	13.8	0.0	58.8	28.5	27.0	29.7
GCMA[72]	81.7	46.9	58.8	22.0	20.0	41.2	40.5	41.6	64.8	31.0	32.1	53.5	47.5	75.5	39.2	0.0	49.6	30.7	21.0	42.0
MGCDA[73]	80.3	49.3	66.2	7.8	11.0	41.4	38.9	39.0	64.1	18.0	55.8	52.1	53.5	74.7	66.0	0.0	37.5	29.1	22.7	42.5
DANNet[74]	90.0	54.0	74.8	41.0	21.1	25.0	26.8	30.2	72.0	26.2	84.0	47.0	33.9	68.2	19.0	0.3	66.4	38.3	23.6	44.3
DAFormer[51]	93.5	65.5	73.3	39.4	19.2	53.3	44.1	44.0	59.5	34.5	66.6	53.4	52.7	82.1	52.7	9.5	89.3	50.5	38.5	53.8
HRDA[52]	90.4	56.3	72.0	39.5	19.5	57.8	52.7	43.1	59.3	29.1	70.5	60.0	58.6	84.0	75.5	11.2	90.5	51.6	40.9	55.9
MIC(HRDA)[68]	94.8	75.0	84.0	55.1	28.4	62.0	35.5	52.6	59.2	46.8	70.0	65.2	61.7	82.1	64.2	18.5	91.3	52.6	44.0	60.2
PGPC+DAFormer	90.4	54.3	81.6	56.3	24.6	60.0	40.0	51.7	42.5	40.0	39.4	62.8	61.7	73.3	72.2	4.3	91.9	49.7	43.9	54.7
PGPC+MIC(DAFormer)	92.5	59.5	79.3	53.5	24.5	60.7	42.6	53.4	42.3	43.9	39.3	63.8	62.6	73.3	71.5	6.0	93.3	52.1	74.3	55.7
PGPC+HRDA	90.9	57.6	79.4	45.3	21.6	60.5	32.2	50.6	56.2	39.8	66.5	63.7	53.7	83.6	70.1	25.0	92.1	56.8	41.2	57.2
PGPC+MIC(HRDA)	94.5	65.7	85.4	54.7	27.5	62.3	56.0	54.8	58.0	47.5	68.8	66.2	65.6	75.5	79.4	4.5	93.2	61.2	45.6	61.3

Table 4: The mIoU % scores of semantic segmentation models trained on Cityscapes and evaluated on the ACDC test dataset. The preeminent scores within columns are highlighted through bold text.

Cityscapes to ACDC																				
Method	road	sidewalk	building	wall	fence	pole	light	sign	veg	terrain	sky	person	rider	car	truck	bus	train	mbike	bike	mIoU
ADVENT[71]	72.9	14.3	40.5	16.6	21.2	9.3	17.4	21.2	63.8	23.8	18.3	32.6	19.5	69.5	36.2	34.5	46.2	26.9	36.1	32.7
GCMA[72]	79.7	48.7	71.5	21.6	29.9	42.5	56.7	57.7	75.8	39.5	87.2	57.4	29.7	80.6	44.9	46.2	62.0	37.2	46.5	53.4
MGCD[73]	73.4	28.7	69.9	19.3	26.3	36.8	53.0	53.3	75.4	32.0	84.6	51.0	26.1	77.6	43.2	45.9	53.9	32.7	41.5	48.7
DANN[74]	84.3	54.2	77.6	38.0	30.0	18.9	41.6	35.2	71.3	39.4	86.6	48.7	29.2	76.2	41.6	43.0	58.6	32.6	43.9	50.0
DAFormer[51]	58.4	51.3	84.0	42.7	35.1	50.7	30.0	57.0	74.8	52.8	51.3	58.3	32.6	82.7	58.3	54.9	82.4	44.1	50.7	55.4
HRDA[52]	88.3	57.9	88.1	55.2	36.7	56.3	62.9	65.3	74.2	57.7	85.9	68.8	45.7	88.5	76.4	82.4	87.7	52.7	60.4	68.0
MIC(HRDA)[68]	90.8	67.1	89.2	54.5	40.5	57.2	62.0	68.4	76.3	61.8	87.0	71.3	49.4	89.7	75.7	86.8	89.1	56.9	63.0	70.4
PGPC+DAFormer	83.2	44.6	83.8	42.5	30.8	48.0	39.0	55.5	68.0	52.2	80.5	57.9	24.0	76.0	51.6	66.0	84.4	39.1	46.7	56.5
PGPC+MIC(DAFormer)	91.6	68.7	86.2	55.7	34.3	54.8	50.6	34.1	73.1	56.9	84.5	65.0	46.4	86.1	67.8	71.4	84.2	52.7	55.9	64.2
PGPC+HRDA	72.0	58.6	88.3	45.9	35.2	52.7	61.0	63.5	77.7	58.0	72.1	66.3	47.0	86.7	67.6	80.7	86.4	48.8	58.3	64.6
PGPC+MIC(HRDA)	85.9	60.1	93.1	63.2	44.0	62.9	71.7	69.1	92.4	41.9	96.9	69.8	30.5	91.3	81.7	89.3	89.0	57.4	66.5	71.4

Table 5: The speed of different models. (*frames/s*)

Method	Training speed	Inference speed
Daformer [51]	0.8	8.9
HRDA [52]	0.4	0.5
PGPC+DAFormer	0.6	2.5
PGPC+HRDA	0.3	0.5

still outperforms pixel-to-pixel (CLUDA: 70.1 mIoU) and pixel-to-prototype (SePiCo: 70.3 mIoU) methods, as elaborated in the introduction section. In an effort to delineate the ramifications of our method in a more illustrative and understandable fashion, we present the visualization [75] of learned feature representations for DAFormer [51] and PGPC, as shown in Fig. 5. Through the visualization, we are able to discern that the clusters formed by the representations of PGPC demonstrate enhanced clarity when compared to those generated by DAFormer [51]. We use circles of different colors in the Fig. 5 to further illustrate the performance of our approach. We can observe that the feature points in our method converge more closely while there are many scattered points in DAFormer [51] by comparing the feature points within these circles. Nevertheless, it is also discernible that certain shortcomings persist in the results. We attribute these shortcomings to erroneous pseudo-labeling, a challenge commonly encountered in unsupervised self-training. Despite our best efforts to minimize the effect of incorrect pseudo-labels, it is currently unavoidable. Eliminating the influence stemming from incorrect pseudo-labels remains a pivotal focus for future research.

Table 6: Effectiveness of the contrastive learning on GTA5 to Cityscapes. SP represents the use of source prototypes as the positive samples. TP means the use of target prototypes as positive samples. SN means the source negative pixels while TN means the target negative pixels. Note that SP and TP cannot be used simultaneously as positive samples.

Method	SP	TP	SN	TN	mIoU	Δ mIoU
PGPC	✓		✓	✓	71.8	+3.5
	✓		✓		70.8	+2.5
	✓			✓	70.0	+1.7
		✓	✓	✓	71.0	+2.7
		✓	✓		70.1	+1.8
		✓		✓	69.8	+1.5
DAFormer					68.3	–

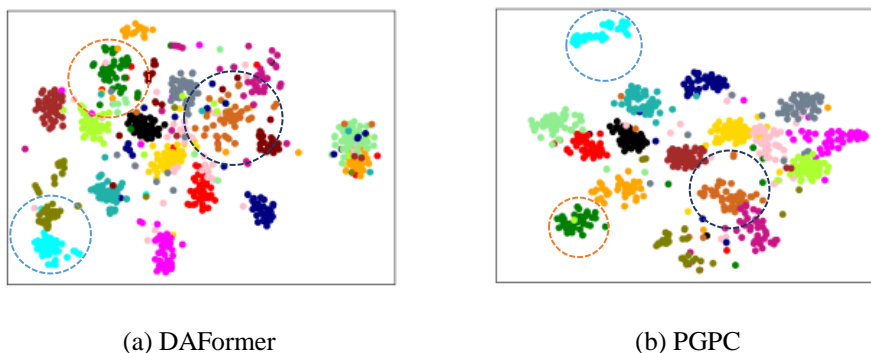


Figure 5: The visualization of our method (PGPC) and DAFormer [51]. Different colors represent distinct categories, and these colors are consistent with the category label colors. We highlight some categories where our method performs better than DAFormer with colored circles.

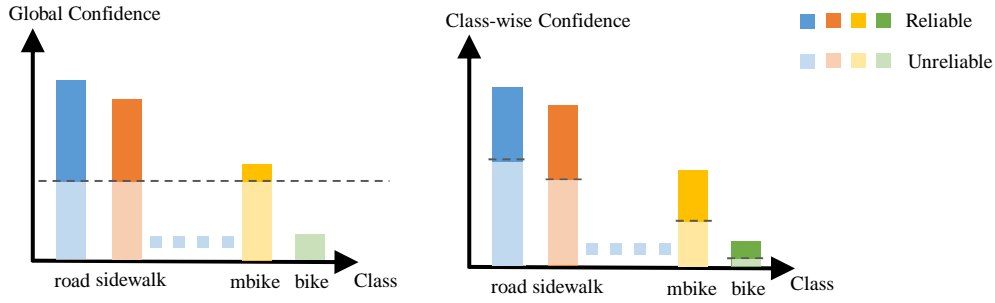


Figure 6: The visualization of global confidence and class-wise confidence methods. Class-wise confidence produces unreliable pseudo-labels for minority classes compared to global confidence, which amplifies noise in contrastive learning and ultimately reduces overall performance.

Table 7: Analysis of the different methods of selecting reliable pixels on GTA5 to Cityscapes.

Method	Global		Class-wise	
	Entropy	Confidence	Entropy	Confidence
mIoU	71.8	70.9	70.9	70.3

Different methods of selecting reliable pixels. In our method, we employ global entropy to select reliable target image pixels, which is a widely used approach [15]. Additionally, there are three other common methods for selecting reliable pixels. One is to directly utilize global confidence [76], and the others takes into account the imbalance in the distribution of different classes, using class-wise confidence or class-wise entropy [29]. The global-based methods select the top $\zeta\%$ with the highest confidence or the lowest entropy from the predictions of all pixels as reliable pixels. In contrast, the class-wise-based methods initially segregate pixels belonging to different classes. Subsequently, for pixels of each class, it selects the top $\zeta\%$ with the highest confidence or the lowest entropy as reliable pixels. To provide a more intuitive illustration of the distinctions between the global-based and class-wise-based methods, we conduct visualizations for global confidence and class-wise confidence, as presented in Fig. 6. We perform experiments with all of these methods, as shown in Table 7. To fairly compare different methods, we conduct multiple experiments with distinct values of $\zeta\%$ and present the best results for each method in the Table 7. We can find that using entropy yields the best results while utilizing class-wise confidence performs the poorest. Although class-wise-based methods are often superior to global-based methods in most research papers [48, 77], they introduce more unreliable pseudo-labels due to the elevated error probability associated with predicting minority classes. The noise is magnified by contrastive learning, leading to a decrease in performance. Furthermore, numerous methods [15, 78] have already indicated that using entropy tends to produce better results compared to confidence, and our experiments align with this viewpoint.

Effectiveness of the target domain loss weight. We train several models to evaluate the weight λ_t in Eq (6), and the result is in Table 8. According to our experiments, the model performs best when $\lambda_t = 1$. This is because the weight of the target domain loss is related to κ , which is an adaptive value. If λ_t is changed, it will significantly reduce the model’s performance.

Effectiveness of the contrastive loss weight. We evaluate how the weight λ_c in Eq. (6) affects the performance of GTA5 to

Cityscapes adaptation. Table 9 reveals the sensitivity of the results to diverse λ_c values. Nonetheless, it is evident that results achieved with varying weights all surpass the baseline performance. We attribute this sensitivity to the imbalance between the contrastive and segmentation loss. The contrastive loss holds a larger magnitude compared to the segmentation loss in our experiments, thus the weight of the contrastive loss significantly influences the overall losses. Through our experiments, we recommend using $\lambda_c = 0.1$ as a default setting.

Table 8: Analysis of the weighting factor λ_t of target domain loss on GTA5 to Cityscapes.

λ_t	0.5	0.8	1.0	1.2	1.5
mIoU	61.25	61.19	71.8	67.49	67.69

Table 9: Analysis of the weighting factor λ_c of contrastive learning loss on GTA5 to Cityscapes. Note that $\lambda_c = 0$ means that the confidence loss is not applied.

λ_c	0	0.05	0.1	0.2	0.3	0.4
mIoU	68.3	70.4	71.8	71.0	70.5	70.2

Effectiveness of the number of anchor pixels and negative samples. Through the modification of the number of anchor pixels and negative samples in our framework, we observe varying results as depicted in Table 10. We find that an increased number of negative samples correlates with improved performance. This is because more negative samples approximate the true distribution more closely. Due to the limitation of computing resources, we take at most 512 negative samples.

Table 10: Analysis of the negative numbers on GTA5 to Cityscapes.

Anchor Numbers	256	256	256	128	512
Negative Numbers	128	256	512	512	512
mIoU	69.9	70.0	71.8	70.0	70.3

Effectiveness of the proportion of reliable pixels. We examine how the proportion of reliable pixels η affects the performance in Table 11. We observe that $\eta = 0.5$ achieves the best result. If η is too large, some incorrect samples may be generated. If η is too small, some high-confidence samples may be ignored.

Effectiveness of the values of r . We tested the performance of the model using Eq. (11) with various values of r , and the results are presented in Table 12. By ranking the probabilities of all categories associated with a particular pixel, if category c falls within the r categories with the lowest probabilities, that pixel is considered as part of the negative sample set. Thus, the value of r significantly impacts the robustness of the model. If the value of r is relatively small, it may introduce noise. Conversely, if r is relatively large, the distance between the pixels in the negative sample set and the target pixel in the feature space will be too far, making it ineffective for training. Based on our experiments, we found that $r = 4$ enables the model to achieve optimal robustness.

Table 11: Analysis of the proportion of reliable pixels on GTA5 to Cityscapes.

η	0	0.4	0.5	0.6	0.7
mIoU	68.3	70.2	71.8	70.5	69.8

Table 12: Analysis of the values of r .

r	3	4	5	6
mIoU	69.7	71.8	69.6	68.7

5. Conclusion

In our study, we propose a novel contrastive learning approach to improve the effectiveness of domain adaptive semantic segmentation. First, we analyze the merits and demerits of existing contrastive learning methods and make improvements to address their limitations. Then, we explore the use of all target pixels to boost model performance, even though a substantial portion of pseudo-labels for target pixels is unreliable. Our method achieved remarkable results on two challenging benchmarks, surpassing previous methods by a significant margin. Extensive ablation studies are conducted to confirm the effectiveness of our approach. Moreover, we illustrate the adaptability of our approach to diverse architectures.

In the future, there are several approaches that can be employed to further enhance our method. First, our method requires a significant amount of computational resources during training, so reducing resource consumption can be considered a viable direction for improvement. Second, our method is still susceptible to errors caused by erroneous pseudo-labels, leading to error accumulation. Therefore, efforts may be directed toward denoising pseudo-labels.

6. Data availability

The datasets analyzed during the current study are available at GTA5 dataset [https://download.visinf.tu-darmstadt.de/data/from_games], Cityscapes dataset [<https://www.cityscapes-dataset.com>], SYNTHIA dataset [<http://adas.cvc.uab.es/synthia>], DarkZurich dataset [<https://www.trace.ethz.ch>], and ACDC dataset [<https://acdc.vision.ee.ethz.ch>].

ACKNOWLEDGMENT

This work was partially supported by the National Key Research and Development Program of China (2021YFB3301303), the National Natural Science Foundation of China (12105105, 62273149), the startup fund from East China University of Science and Technology under Grant JKH01241603 and the Programme of Introducing Talents of Discipline to Universities (the 111 Project) under Grant B17017.

References

- [1] O. Ronneberger, P. Fischer, T. Brox, U-net: Convolutional networks for biomedical image segmentation, in: Medical Image Computing and Computer-Assisted Intervention–MICCAI 2015: 18th International Conference, Munich, Germany, October 5-9, 2015, Proceedings, Part III 18, Springer, 2015, pp. 234–241.
- [2] R. Zurbrügg, H. Blum, C. Cadena, R. Siegart, L. Schmid, Embodied active domain adaptation for semantic segmentation via informative path planning, *IEEE Robotics and Automation Letters* 7 (4) (2022) 8691–8698.
- [3] E. Yurtsever, J. Lambert, A. Carballo, K. Takeda, A survey of autonomous driving: Common practices and emerging technologies, *IEEE access* 8 (2020) 58443–58469.
- [4] Chen, Liang-Chieh and Papandreou, George and Kokkinos, Iasonas and Murphy, Kevin and Yuille, Alan L, Deeplab: Semantic image segmentation with deep convolutional nets, atrous convolution, and fully connected crfs, *IEEE transactions on pattern analysis and machine intelligence* 40 (4) (2017) 834–848.
- [5] L.-C. Chen, G. Papandreou, F. Schroff, H. Adam, Rethinking atrous convolution for semantic image segmentation, *arXiv preprint arXiv:1706.05587* (2017).
- [6] Y. Li, L. Song, Y. Chen, Z. Li, X. Zhang, X. Wang, J. Sun, Learning dynamic routing for semantic segmentation, in: Proceedings of the IEEE/CVF Conference on Computer Vision and Pattern Recognition, 2020, pp. 8553–8562.
- [7] J. Fan, F. Wang, H. Chu, X. Hu, Y. Cheng, B. Gao, Mlfnet: Multi-level fusion network for real-time semantic segmentation of autonomous driving, *IEEE Transactions on Intelligent Vehicles* 8 (1) (2023) 756–767. doi:10.1109/TIV.2022.3176860.
- [8] D. Sun, G. Gao, L. Huang, Y. Liu, D. Liu, Extraction of water bodies from high-resolution remote sensing imagery based on a deep semantic segmentation network, *Scientific Reports* 14 (1) (2024) 14604.
- [9] L. Lu, Y. Xiao, X. Chang, X. Wang, P. Ren, Z. Ren, Deformable attention-oriented feature pyramid network for semantic segmentation, *Knowledge-Based Systems* 254 (2022) 109623.
- [10] S. Zheng, J. Lu, H. Zhao, X. Zhu, Z. Luo, Y. Wang, Y. Fu, J. Feng, T. Xiang, P. H. Torr, et al., Rethinking semantic segmentation from a sequence-to-sequence perspective with transformers, in: Proceedings of the IEEE/CVF conference on computer vision and pattern recognition, 2021, pp. 6881–6890.
- [11] E. Xie, W. Wang, Z. Yu, A. Anandkumar, J. M. Alvarez, P. Luo, Segformer: Simple and efficient design for semantic segmentation with transformers, *Advances in Neural Information Processing Systems* 34 (2021) 12077–12090.
- [12] Y. Miao, Y. Sun, Y. Zhang, J. Wang, X. Zhang, An efficient point cloud semantic segmentation network with multiscale super-patch transformer, *Scientific Reports* 14 (1) (2024) 14581.
- [13] S. R. Richter, V. Vineet, S. Roth, V. Koltun, Playing for data: Ground truth from computer games, in: European conference on computer vision, Springer, 2016, pp. 102–118.
- [14] G. Ros, L. Sellart, J. Materzynska, D. Vazquez, A. M. Lopez, The synthia dataset: A large collection of synthetic images for semantic segmentation of urban scenes, in: Proceedings of the IEEE conference on computer vision and pattern recognition, 2016, pp. 3234–3243.
- [15] Z. Yan, X. Yu, Y. Qin, Y. Wu, X. Han, S. Cui, Pixel-level intra-domain adaptation for semantic segmentation, in: Proceedings of the 29th ACM International Conference on Multimedia, 2021, pp. 404–413.
- [16] X. Huo, L. Xie, H. Hu, W. Zhou, H. Li, Q. Tian, Domain-agnostic prior for transfer semantic segmentation, in: Proceedings of the IEEE/CVF Conference on Computer Vision and Pattern Recognition, 2022, pp. 7075–7085.
- [17] Y. Wang, J. Peng, Z. Zhang, Uncertainty-aware pseudo label refinery for domain adaptive semantic segmentation, in: 2021 IEEE/CVF International Conference on Computer Vision (ICCV), 2021, pp. 9072–9081. doi:10.1109/ICCV48922.2021.00896.
- [18] M. Liao, S. Tian, Y. Zhang, G. Hua, W. Zou, X. Li, Pda: Progressive domain adaptation for semantic segmentation, *Knowledge-Based Systems* 284 (2024) 111179.
- [19] Y. Zhang, M. Ye, Y. Gan, W. Zhang, Knowledge based domain adaptation for semantic segmentation, *Knowledge-Based Systems* 193 (2020) 105444.
- [20] C.-X. Ren, Y.-H. Liu, X.-W. Zhang, K.-K. Huang, Multi-source unsupervised domain adaptation via pseudo target domain, *IEEE Transactions on Image Processing* 31 (2022) 2122–2135.
- [21] H. Lin, Y. Zhang, Z. Qiu, S. Niu, C. Gan, Y. Liu, M. Tan, Prototype-guided continual adaptation for class-incremental unsupervised domain adaptation, in:

- European Conference on Computer Vision, Springer, 2022, pp. 351–368.
- [22] Y. Yang, D. Lao, G. Sundaramoorthi, S. Soatto, Phase consistent ecological domain adaptation, in: Proceedings of the IEEE/CVF Conference on Computer Vision and Pattern Recognition, 2020, pp. 9011–9020.
- [23] C. Corbière, N. Thome, A. Saporta, T.-H. Vu, M. Cord, P. Pérez, Confidence estimation via auxiliary models, *IEEE Transactions on Pattern Analysis and Machine Intelligence* 44 (10) (2021) 6043–6055.
- [24] N. Araslanov, S. Roth, Self-supervised augmentation consistency for adapting semantic segmentation, in: Proceedings of the IEEE/CVF Conference on Computer Vision and Pattern Recognition, 2021, pp. 15384–15394.
- [25] H. Xu, M. Yang, L. Deng, Y. Qian, C. Wang, Neutral cross-entropy loss based unsupervised domain adaptation for semantic segmentation, *IEEE Transactions on Image Processing* 30 (2021) 4516–4525.
- [26] M. Vayyat, J. Kasi, A. Bhattacharya, S. Ahmed, R. Tallamraju, Cluda: Contrastive learning in unsupervised domain adaptation for semantic segmentation, arXiv preprint arXiv:2208.14227 (2022).
- [27] S. Chopra, R. Hadsell, Y. LeCun, Learning a similarity metric discriminatively, with application to face verification, in: 2005 IEEE Computer Society Conference on Computer Vision and Pattern Recognition (CVPR'05), Vol. 1, IEEE, 2005, pp. 539–546.
- [28] B. Xie, S. Li, M. Li, C. H. Liu, G. Huang, G. Wang, Sepico: Semantic-guided pixel contrast for domain adaptive semantic segmentation, *IEEE Transactions on Pattern Analysis and Machine Intelligence* (2023).
- [29] Z. Jiang, Y. Li, C. Yang, P. Gao, Y. Wang, Y. Tai, C. Wang, Prototypical contrast adaptation for domain adaptive semantic segmentation, in: Computer Vision–ECCV 2022: 17th European Conference, Tel Aviv, Israel, October 23–27, 2022, Proceedings, Part XXXIV, Springer, 2022, pp. 36–54.
- [30] J. Huang, D. Guan, A. Xiao, S. Lu, L. Shao, Category contrast for unsupervised domain adaptation in visual tasks, in: Proceedings of the IEEE/CVF Conference on Computer Vision and Pattern Recognition, 2022, pp. 1203–1214.
- [31] G. Lee, C. Eom, W. Lee, H. Park, B. Ham, Bi-directional contrastive learning for domain adaptive semantic segmentation, in: Computer Vision–ECCV 2022: 17th European Conference, Tel Aviv, Israel, October 23–27, 2022, Proceedings, Part XXX, Springer, 2022, pp. 38–55.
- [32] E. Arazo, D. Ortego, P. Albert, N. E. O'Connor, K. McGuinness, Pseudo-labeling and confirmation bias in deep semi-supervised learning, in: 2020 International Joint Conference on Neural Networks (IJCNN), IEEE, 2020, pp. 1–8.
- [33] E. Shelhamer, J. Long, T. Darrell, Fully convolutional networks for semantic segmentation, *IEEE Transactions on Pattern Analysis and Machine Intelligence* 39 (4) (2017) 640–651. doi:10.1109/TPAMI.2016.2572683.
- [34] H. Zhao, J. Shi, X. Qi, X. Wang, J. Jia, Pyramid scene parsing network, in: Proceedings of the IEEE conference on computer vision and pattern recognition, 2017, pp. 2881–2890.
- [35] F. Yu, V. Koltun, Multi-scale context aggregation by dilated convolutions, arXiv preprint arXiv:1511.07122 (2015).
- [36] Y. Yuan, X. Chen, J. Wang, Object-contextual representations for semantic segmentation, in: Computer Vision–ECCV 2020: 16th European Conference, Glasgow, UK, August 23–28, 2020, Proceedings, Part VI 16, Springer, 2020, pp. 173–190.
- [37] J. Fu, J. Liu, H. Tian, Y. Li, Y. Bao, Z. Fang, H. Lu, Dual attention network for scene segmentation, in: Proceedings of the IEEE/CVF conference on computer vision and pattern recognition, 2019, pp. 3146–3154.
- [38] L. Huang, Y. Yuan, J. Guo, C. Zhang, X. Chen, J. Wang, Interlaced sparse self-attention for semantic segmentation, arXiv preprint arXiv:1907.12273 (2019).
- [39] A. Vaswani, N. Shazeer, N. Parmar, J. Uszkoreit, L. Jones, A. N. Gomez, Ł. Kaiser, I. Polosukhin, Attention is all you need, *Advances in neural information processing systems* 30 (2017).
- [40] A. Dosovitskiy, L. Beyer, A. Kolesnikov, D. Weissenborn, X. Zhai, T. Unterthiner, M. Dehghani, M. Minderer, G. Heigold, S. Gelly, et al., An image is worth 16x16 words: Transformers for image recognition at scale, arXiv preprint arXiv:2010.11929 (2020).
- [41] Z. Liu, Y. Lin, Y. Cao, H. Hu, Y. Wei, Z. Zhang, S. Lin, B. Guo, Swin transformer: Hierarchical vision transformer using shifted windows, in: Proceedings of the IEEE/CVF international conference on computer vision, 2021, pp. 10012–10022.
- [42] J. Hoffman, D. Wang, F. Yu, T. Darrell, Fcns in the wild: Pixel-level adversarial and constraint-based adaptation, arXiv preprint arXiv:1612.02649 (2016).
- [43] J. Hoffman, E. Tzeng, T. Park, J.-Y. Zhu, P. Isola, K. Saenko, A. Efros, T. Darrell, Cycada: Cycle-consistent adversarial domain adaptation, in: International

- conference on machine learning, PMLR, 2018, pp. 1989–1998.
- [44] M. Kim, H. Byun, Learning texture invariant representation for domain adaptation of semantic segmentation, in: Proceedings of the IEEE/CVF conference on computer vision and pattern recognition, 2020, pp. 12975–12984.
- [45] K. Mei, C. Zhu, J. Zou, S. Zhang, Instance adaptive self-training for unsupervised domain adaptation, in: European conference on computer vision, Springer, 2020, pp. 415–430.
- [46] Y. Zou, Z. Yu, X. Liu, B. Kumar, J. Wang, Confidence regularized self-training, in: Proceedings of the IEEE/CVF International Conference on Computer Vision, 2019, pp. 5982–5991.
- [47] K. Sohn, D. Berthelot, N. Carlini, Z. Zhang, H. Zhang, C. A. Raffel, E. D. Cubuk, A. Kurakin, C.-L. Li, Fixmatch: Simplifying semi-supervised learning with consistency and confidence, *Advances in neural information processing systems* 33 (2020) 596–608.
- [48] L. Gao, J. Zhang, L. Zhang, D. Tao, Dsp: Dual soft-paste for unsupervised domain adaptive semantic segmentation, in: Proceedings of the 29th ACM International Conference on Multimedia, 2021, pp. 2825–2833.
- [49] L. Hoyer, D. Dai, Q. Wang, Y. Chen, L. Van Gool, Improving semi-supervised and domain-adaptive semantic segmentation with self-supervised depth estimation, *arXiv preprint arXiv:2108.12545* (2021).
- [50] R. Gong, Q. Wang, M. Danelljan, D. Dai, L. Van Gool, Continuous pseudo-label rectified domain adaptive semantic segmentation with implicit neural representations, in: Proceedings of the IEEE/CVF Conference on Computer Vision and Pattern Recognition, 2023, pp. 7225–7235.
- [51] L. Hoyer, D. Dai, L. Van Gool, Daformer: Improving network architectures and training strategies for domain-adaptive semantic segmentation, in: Proceedings of the IEEE/CVF Conference on Computer Vision and Pattern Recognition, 2022, pp. 9924–9935.
- [52] L. Hoyer, D. Dai, L. Van Gool, Hrrda: Context-aware high-resolution domain-adaptive semantic segmentation, in: *Computer Vision–ECCV 2022: 17th European Conference, Tel Aviv, Israel, October 23–27, 2022, Proceedings, Part XXX*, Springer, 2022, pp. 372–391.
- [53] T. Chen, S. Kornblith, K. Swersky, M. Norouzi, G. E. Hinton, Big self-supervised models are strong semi-supervised learners, *Advances in neural information processing systems* 33 (2020) 22243–22255.
- [54] X. Chen, S. Xie, K. He, An empirical study of training self-supervised vision transformers, in: Proceedings of the IEEE/CVF International Conference on Computer Vision, 2021, pp. 9640–9649.
- [55] J.-B. Grill, F. Strub, F. Altché, C. Tallec, P. Richemond, E. Buchatskaya, C. Doersch, B. Avila Pires, Z. Guo, M. Gheshlaghi Azar, et al., Bootstrap your own latent—a new approach to self-supervised learning, *Advances in neural information processing systems* 33 (2020) 21271–21284.
- [56] H. Hu, J. Cui, L. Wang, Region-aware contrastive learning for semantic segmentation, in: Proceedings of the IEEE/CVF International Conference on Computer Vision, 2021, pp. 16291–16301.
- [57] Y. Zhong, B. Yuan, H. Wu, Z. Yuan, J. Peng, Y.-X. Wang, Pixel contrastive-consistent semi-supervised semantic segmentation, in: Proceedings of the IEEE/CVF International Conference on Computer Vision, 2021, pp. 7273–7282.
- [58] X. Lai, Z. Tian, L. Jiang, S. Liu, H. Zhao, L. Wang, J. Jia, Semi-supervised semantic segmentation with directional context-aware consistency, in: Proceedings of the IEEE/CVF Conference on Computer Vision and Pattern Recognition, 2021, pp. 1205–1214.
- [59] Y. Wang, H. Wang, Y. Shen, J. Fei, W. Li, G. Jin, L. Wu, R. Zhao, X. Le, Semi-supervised semantic segmentation using unreliable pseudo-labels, in: Proceedings of the IEEE/CVF Conference on Computer Vision and Pattern Recognition, 2022, pp. 4248–4257.
- [60] W. Wang, T. Zhou, F. Yu, J. Dai, E. Konukoglu, L. Van Gool, Exploring cross-image pixel contrast for semantic segmentation, in: Proceedings of the IEEE/CVF International Conference on Computer Vision, 2021, pp. 7303–7313.
- [61] A. v. d. Oord, Y. Li, O. Vinyals, Representation learning with contrastive predictive coding, *arXiv preprint arXiv:1807.03748* (2018).
- [62] X. Chen, H. Fan, R. Girshick, K. He, Improved baselines with momentum contrastive learning, *arXiv preprint arXiv:2003.04297* (2020).
- [63] M. Cordts, M. Omran, S. Ramos, T. Rehfeld, M. Enzweiler, R. Benenson, U. Franke, S. Roth, B. Schiele, The cityscapes dataset for semantic urban scene understanding, in: Proceedings of the IEEE conference on computer vision and pattern recognition, 2016, pp. 3213–3223.
- [64] J. Deng, W. Dong, R. Socher, L.-J. Li, K. Li, L. Fei-Fei, Imagenet: A large-scale hierarchical image database, in: 2009 IEEE conference on computer vision and pattern recognition, Ieee, 2009, pp. 248–255.
- [65] M. Contributors, Mmsegmentation: Openmmlab semantic segmentation toolbox and benchmark, <https://github.com/openmmlab/msegmentation>

(2020).

- [66] I. Loshchilov, F. Hutter, Decoupled weight decay regularization, arXiv preprint arXiv:1711.05101 (2017).
- [67] P. Zhang, B. Zhang, T. Zhang, D. Chen, Y. Wang, F. Wen, Prototypical pseudo label denoising and target structure learning for domain adaptive semantic segmentation, in: Proceedings of the IEEE/CVF conference on computer vision and pattern recognition, 2021, pp. 12414–12424.
- [68] L. Hoyer, D. Dai, H. Wang, L. Van Gool, Mic: Masked image consistency for context-enhanced domain adaptation, in: Proceedings of the IEEE/CVF Conference on Computer Vision and Pattern Recognition, 2023, pp. 11721–11732.
- [69] W. Tranheden, V. Olsson, J. Pinto, L. Svensson, Dacs: Domain adaptation via cross-domain mixed sampling, in: Proceedings of the IEEE/CVF Winter Conference on Applications of Computer Vision, 2021, pp. 1379–1389.
- [70] N. Araslanov, S. Roth, Self-supervised augmentation consistency for adapting semantic segmentation, in: Proceedings of the IEEE/CVF Conference on Computer Vision and Pattern Recognition, 2021, pp. 15384–15394.
- [71] T.-H. Vu, H. Jain, M. Bucher, M. Cord, P. Pérez, Advent: Adversarial entropy minimization for domain adaptation in semantic segmentation, Proceedings / CVPR, IEEE Computer Society Conference on Computer Vision and Pattern Recognition (2019) 2517–2526.
- [72] C. Sakaridis, D. Dai, L. V. Gool, Guided curriculum model adaptation and uncertainty-aware evaluation for semantic nighttime image segmentation, in: Proceedings of the IEEE/CVF international conference on computer vision, 2019, pp. 7374–7383.
- [73] C. Sakaridis, D. Dai, L. Van Gool, Map-guided curriculum domain adaptation and uncertainty-aware evaluation for semantic nighttime image segmentation, IEEE Transactions on Pattern Analysis and Machine Intelligence 44 (6) (2020) 3139–3153.
- [74] X. Wu, Z. Wu, H. Guo, L. Ju, S. Wang, Dattet: A one-stage domain adaptation network for unsupervised nighttime semantic segmentation, in: Proceedings of the IEEE/CVF Conference on Computer Vision and Pattern Recognition, 2021, pp. 15769–15778.
- [75] L. Van der Maaten, G. Hinton, Visualizing data using t-sne., Journal of machine learning research 9 (11) (2008).
- [76] Y. Li, L. Yuan, N. Vasconcelos, Bidirectional learning for domain adaptation of semantic segmentation, in: Proceedings of the IEEE/CVF Conference on Computer Vision and Pattern Recognition, 2019, pp. 6936–6945.
- [77] Y. Zou, Z. Yu, B. Kumar, J. Wang, Unsupervised domain adaptation for semantic segmentation via class-balanced self-training, in: Proceedings of the European conference on computer vision (ECCV), 2018, pp. 289–305.
- [78] A. Saporta, T.-H. Vu, M. Cord, P. Pérez, Esl: Entropy-guided self-supervised learning for domain adaptation in semantic segmentation, arXiv preprint arXiv:2006.08658 (2020).